Turnip Mosaic Virus Components Are Released into the Extracellular Space by Vesicles in Infected Leaves[1]

Nooshin Movahed,[a,2] Daniel Garcia Cabanillas,[b,2] Juan Wan,[c] Hojatollah Vali,[d,e] Jean-François Laliberté,[b] and Huanquan Zheng[a,3,4]

[a]Department of Biology, McGill University, Montréal, Québec, H3A 1B1, Canada
[b]Institut National de la Recherche Scientifique-Institut Armand-Frappier, Laval, Québec, H7V 1B7, Canada
[c]Department of Plant and Microbial Biology, University of California, Berkeley, California 94720
[d]Facility for Electron Microscopy Research, McGill University, Montréal, Québec, H3A 0C7, Canada
[e]Department of Anatomy & Cell Biology, McGill University, Montréal, Québec, H3A 0C7, Canada

ORCID IDs: 0000-0001-8852-245X (N.M.); 0000-0003-1465-9941 (D.G.C.); 0000-0002-6187-5113 (J.W.); 0000-0002-6934-224X (J.-F.L.); 0000-0003-2986-725X (H.Z.).

Turnip mosaic virus (TuMV) reorganizes the endomembrane system of the infected cell to generate endoplasmic-reticulum–derived motile vesicles containing viral replication complexes. The membrane-associated viral protein $6K_2$ plays a key role in the formation of these vesicles. Using confocal microscopy, we observed that this viral protein, a marker for viral replication complexes, localized in the extracellular space of infected *Nicotiana benthamiana* leaves. Previously, we showed that viral RNA is associated with multivesicular bodies (MVBs). Here, using transmission electron microscopy, we observed the proliferation of MVBs during infection and their fusion with the plasma membrane that resulted in the release of their intraluminal vesicles in the extracellular space. Immunogold labeling with a monoclonal antibody that recognizes double-stranded RNA indicated that the released vesicles contained viral RNA. Focused ion beam-extreme high-resolution scanning electron microscopy was used to generate a three-dimensional image that showed extracellular vesicles in the cell wall. The presence of TuMV proteins in the extracellular space was confirmed by proteomic analysis of purified extracellular vesicles from *N. benthamiana* and Arabidopsis (*Arabidopsis thaliana*). Host proteins involved in biotic defense and in interorganelle vesicular exchange were also detected. The association of extracellular vesicles with viral proteins and RNA emphasizes the implication of the plant extracellular space in viral infection.

Proteins found in the extracellular space of eukaryotic cells are either secreted by exocytosis or through the release of extracellular vesicles. Extracellular vesicles are produced in a wide variety of shapes and have been classified into at least three groups according to their size (György et al., 2011; Akers et al., 2013; Abels and Breakefield, 2016; Dreyer and Baur, 2016). The largest vesicles are known as apoptotic bodies, which have diameters of >1 μm. The other two classes are microvesicles (100–1000-nm in diameter) and exosomes (30–150 nm in diameter). Microvesicles are shed directly from the plasma membrane, whereas exosomes are released after the fusion of a multivesicular body (MVB) with the plasma membrane. Exosomes were long considered as sample processing artifacts or as fragments of dying cells undergoing apoptosis. Increasing interest on those extracellular vesicles has revealed their implication in many biological processes. For instance, extracellular vesicles purified from different extracellular fluids, such as blood, urine, and amniotic fluid, were shown to transport proteins and different types of RNAs such as mRNAs and micro RNA (Bern, 2017; Ciregia et al., 2017; Fleshner and Crane, 2017; Lawson et al., 2017; Xu et al., 2017). It was recently discovered that many mammalian positive-sense (+) RNA viruses use exosomes to modulate the cell immune response (Masciopinto et al., 2004; Canitano et al., 2013; Arenaccio et al., 2014; Longatti, 2015; Ahsan et al., 2016; Kouwaki et al., 2016; Xu et al., 2017). Furthermore, nonenveloped viruses were thought to exit cells exclusively by inducing their lysis. However, it was recently shown that some of them are able to transiently acquire a membrane envelope and generate secondary infection foci by transporting their viral RNA (vRNA) or their viral particles

[1]This work was supported by the Natural Sciences and Engineering Research Council of Canada and Fonds de Recherche du Québec sur la Nature et les Technologies (grants to J.-F.L. and H.Z.).

[2]These authors contributed equally to this article.

[3]Author for contact: hugo.zheng@mcgill.ca.

[4]Senior author.

The author responsible for distribution of materials integral to the findings presented in this article in accordance with the policy described in the Instructions for Authors (www.plantphysiol.org) is: Huanquan Zheng (hugo.zheng@mcgill.ca).

H.V., J.-F.L., and H.Z. supervised the experiments; N.M. and D.G.C. performed all experiments; J.W. provided initial data to N.M. and D.G.C.; N.M. and D.G.C. designed the experiments and analyzed the data; N.M. and D.G.C. conceived the project and wrote the article with contributions of all the authors; J.-F.L. and H.Z. supervised and completed the writing.

www.plantphysiol.org/cgi/doi/10.1104/pp.19.00381

(Bukong et al., 2014) in extracellular vesicles through long distances in the extracellular fluids (Masciopinto et al., 2004; Canitano et al., 2013; Feng et al., 2013; Arenaccio et al., 2014; Bukong et al., 2014; Longatti, 2015; Ahsan et al., 2016; Yang et al., 2017).

Information concerning plant-cell–derived extracellular vesicles is rather limited, perhaps because of the difficulty in obtaining large quantities of extracellular apoplastic fluid enriched in exosomes and microvesicles. Most of the available information about plant exosomes highlights the implication of the SNARE SYP121 (PENETRATION1 [PEN1]) protein and comes from studies of plant–fungi interactions and more recently from plant–bacteria interactions (Nielsen et al., 2012; Rutter and Innes, 2017; Cai et al., 2018). Accumulating evidence suggests that plant extracellular vesicles transport small nucleic acids (e.g. small interfering RNA, micro RNA) in different contexts as their mammalian counterpart (Cai et al., 2018; Baldrich et al., 2019). They also carry other specific materials (e.g. proteins) in the extracellular space of the plant to accomplish still undiscovered functions (An et al., 2006b; Regente et al., 2009; Wang et al., 2010; Rutter and Innes, 2017; Cai et al., 2018). An improved extraction protocol has been described for obtaining extracellular vesicles from Arabidopsis (*Arabidopsis thaliana*; Rutter and Innes, 2017). Proteomic analyses of the extracellular vesicles obtained with this procedure indicated that they are enriched in proteins involved in biotic and abiotic stress responses, suggesting that extracellular vesicles may have a role in plant immune responses. Despite the similarities between pathogenic +RNA viruses across kingdoms, there is no information linking plant extracellular vesicles with viruses. The only investigation on the subject is the release of Rice Dwarf Virus from insect vector cells, which involves exosomes derived from MVBs (Wei et al., 2009)

Turnip Mosaic Virus (TuMV) is a +RNA virus that belongs to the order *Picornavirales*. The 9.8-kb genome encodes a polyprotein that is proteolytically processed into at least 11 viral proteins. +RNA viruses reorganize the endomembrane system to generate quasi-organelle structures called "viral factories" (Laliberté and Zheng, 2014). In the case of TuMV, these factories are motile vesicles of ~100 nm in diameter that contain the TuMV genome as well as viral and host proteins involved in vRNA replication (Cotton et al., 2009). These motile vesicles move intercellularly from infected cells to adjacent healthy cells through virus-modified plasmodesmata until they reach the vascular tissues (Grangeon et al., 2012, 2013; Agbeci et al., 2013). Interestingly, replication vesicles were found in xylem vessels (Wan and Laliberté, 2015), which challenges the general belief that viral replication complexes are found exclusively inside infected cells.

The membrane-associated viral protein $6K_2$ plays a key role in the formation of viral replication vesicles (Restrepo-Hartwig and Carrington, 1994). It interacts with the coatomer protein II Sec24A protein, which allows the release of replication vesicles at endoplasmic reticulum exit sites (Jiang et al., 2015). Replication vesicles then bypass the Golgi apparatus and are associated with the prevacuolar compartment/MVB SNARE Vti11 (Cabanillas et al., 2018). Of particular interest is the finding that Vti11 is associated with Arabidopsis extracellular vesicles (Rutter and Innes, 2017).

In this study, we revealed that TuMV components could be released in the extracellular space of infected *Nicotiana benthamiana* and Arabidopsis leaves and that they are linked to extracellular vesicles. Transmission electron microscopy (TEM) immuno-gold labeling and focused ion beam-extreme high-resolution scanning electron microscopy (FIB-EHRSEM) on *N. benthamiana* leaves showed abundant MVBs releasing intraluminal vesicles containing vRNA into the extracellular space and penetrating the cell wall. Proteomic analyses of purified extracellular vesicles from *N. benthamiana* and Arabidopsis revealed the presence of viral proteins together with host factors, many of them involved in plant immune response. This discovery challenges the notion that no viral components, besides viral particles, are found outside of plant cells and highlights the implication of extracellular vesicles in viral infection.

RESULTS

$6K_2$ Is Observed in the Extracellular Space of TuMV-Infected Leaves

Recently, we reported that the trafficking of the replication vesicles of TuMV requires MVB SNARE Vti11 (Cabanillas et al., 2018). Because Vti11 is also found in Arabidopsis extracellular vesicles (Rutter and Innes, 2017), we therefore wondered if TuMV components could be released in the extracellular space of infected leaves. *N. benthamiana* leaves were first agroinfiltrated with a suspension of *Agrobacterium tumefaciens* containing the infectious clone pCambiaTuMV/$6K_2$:GFP (Cotton et al., 2009). In this infectious clone, the $6K_2$:GFP coding sequence is inserted between the P1 and HC-Pro cistrons in the TuMV genome and the fusion protein is released from the polyprotein during viral replication. $6K_2$:GFP was also shown to be a marker for membrane-enclosed viral replication complexes (Cotton et al., 2009; Grangeon et al., 2012; Wan et al., 2015). Six days after infiltration (dpi), infected cells were observed by confocal microscopy. The plasma membrane was stained with the FM4-64 dye to delineate the extracellular space between neighboring cells (Fig. 1A). Mainly detected as dispersed punctae within cells, $6K_2$:GFP were also found in the extracellular space (Fig. 1A, white rectangle). A three-dimensional (3D) image of Figure 1B was reconstructed using the image analysis software Imaris (https://imaris.oxinst.com/) and is shown in Figure 1, C and D. This reconstruction shows the presence in the extracellular space of one large $6K_2$ structure of 1.5 μm in length. This large structure is likely a cluster of $6K_2$ punctae, as was previously observed in the xylem of TuMV infected plants (Wan et al., 2015). There was no overlap between

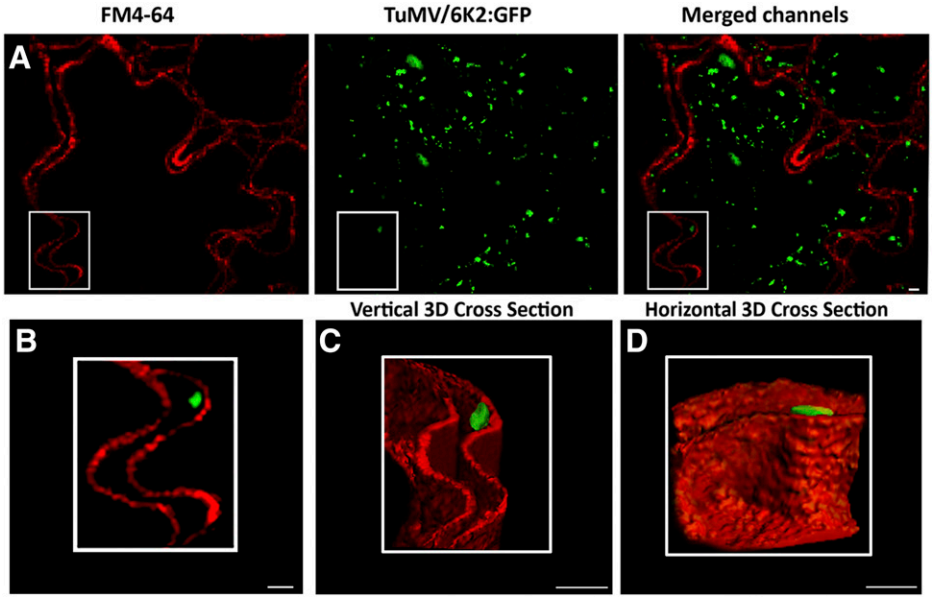

Figure 1. $6K_2$ observed in the intercellular space of TuMV-infected leaves. *N. benthamiana* leaves were agroinfiltrated with *A. tumefaciens* containing pCambiaTuMV/$6K_2$:GFP and observed by confocal microscopy at 6 dpi. A, Left, plasma membrane stained with FM4-64; middle, expression of $6K_2$:GFP; right, merged image. B, Enlargement of the boxed region of the image in (A), which has been used for 3D reconstruction shown in (C) and (D). Scale bars = 2 μm.

the green and the red signals, indicating that the release of $6K_2$ in the extracellular space does not involve fusion of the lipids embedding $6K_2$ with the plasma membrane.

Numerous Vesicular Structures Are Present in the Extracellular Space of TuMV-Infected Leaves

To study the extracellular space of TuMV infected leaves in detail as well as to confirm the confocal observation, sections of TuMV-infected *N. benthamiana* leaves were processed for TEM. We observed numerous circular vesicular structures of 60–150-nm in diameter in the extracellular space of TuMV-infected leaves (Fig. 2A, arrows). Although extracellular vesicular structures were also observed in mock-infected leaves (Fig. 2B), they were statistically found less frequently than in infected leaves (Fig. 2E). We further observed several MVBs fusing with the plasma membrane in TuMV-infected samples (Fig. 2C). Figure 2D shows a close-up view of a fusion event of one MVB with its intraluminal vesicles apparently being released into the extracellular space during TuMV infection. The occurrence of cells with MVBs fusing with the plasma membrane was quantified and was found to take place at a higher frequency in TuMV-infected cells than in mock-infected cells (Fig. 2F).

Multivesicular Bodies and Extracellular Vesicular Structures Contain vRNA

To determine if the extracellular vesicular structures are related to TuMV, we performed immuno-gold labeling using the J2 anti-double stranded RNA (dsRNA) monoclonal antibody that recognizes vRNA. The validity of using the anti-dsRNA J2 monoclonal antibody for labeling vRNA of TuMV was demonstrated in Cotton et al. (2009) and Wan et al. (2015). The RNA signal was always associated with $6K_2$ vesicles during infection, and no background noise was observed in mock conditions or unrelated to viral factories during infection in Wan et al. (2015). At 6 dpi, a limited number of gold particles were found in cells of mock-infected samples (Fig. 3A). However, in TuMV-infected samples, gold particles were abundantly decorating intracellular single membrane vesicular structures and MVBs (Fig. 3B). Additionally, MVBs fusing with the plasma membrane and releasing their intraluminal vesicular structures as well as extracellular vesicular structures were labeled with gold particles (Fig. 3C). Quantification of gold particles per μm^2 in mock- and TuMV-infected samples showed that mock-infected sections did not show any significant labeling as compared to TuMV-infected sections (Fig. 3D).

Extracellular Vesicles Are Found in the Cell Wall of TuMV-Infected Leaves

Although it was proposed that the extracellular vesicles of TuMV move in the paramural space, how they move through the cell wall is not clear (Wan and Laliberté, 2015). In our TEM-based analysis, we found that the extracellular vesicular structures were not only present in the extracellular space, but also apparently within the cell wall during TuMV infection (Fig. 4A). FIB-EHRSEM, which is capable of serially imaging cells at spatial resolutions approximately an order-of-magnitude higher than those currently achieved with optical microscopy, was then used for a 3D reconstruction to examine if the circular configuration of vesicular structures observed is spherical. We collected 250 slices of 7 nm represented in Figure 4B. A 3D reconstruction and a spatial analysis based on these images were then carried out (Fig. 4C; Supplemental Movie S1). Clusters of vesicles (in blue) associated with viral cylindrical

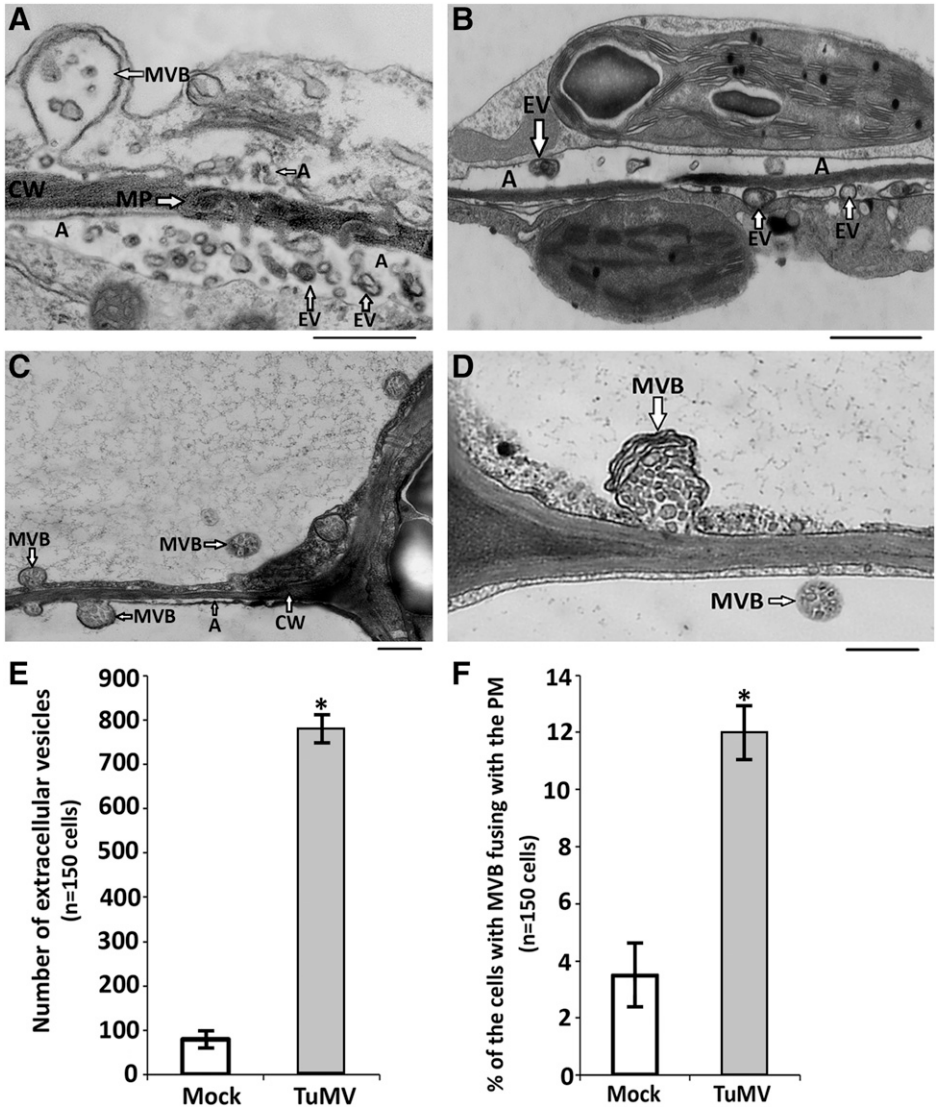

Figure 2. Extracellular vesicles present in the intercellular space of TuMV-infected leaves. *N. benthamiana* leaves were agroinfiltrated with *A. tumefaciens* containing pCambiaTuMV/6K$_2$:GFP or empty pCambia and processed for TEM at 6 dpi. A, Extracellular vesicles and one MVB fusing with the plasma membrane in a TuMV-infected cell. B, Extracellular vesicles in mock-infected samples. C, Low magnification image of MVBs fusing with the plasma membrane in a TuMV-infected section. D, Fusion event with intraluminal vesicles from one MVB being released in the extracellular space during TuMV infection. Scale bars = 500 nm. E, Quantification of the extracellular vesicles observed in mock- and TuMV-infected cells; each error bar = ±SD. F, Quantification of cells showing MVBs fusing with the plasma membrane during mock and TuMV infection; each error bar = ±SD. Asterisks indicate significant difference is found (Student's *t* test, $n = 150$, P value < 0.05). A, apoplast; CW, cell wall; EV, extracellular vesicle; MP, modified plasmodesmata.

inclusion bodies (in magenta; Movahed et al., 2017) and apposed to the plasma membrane (in green) can be seen in both cells (Fig. 4C). An extracellular vesicle in the extracellular space (cream color) was also viewed (Fig. 4C), whereas several distorted vesicles (in blue) in the cell wall (brown) were visible (Fig. 4C). This result confirmed that the extracellular vesicular structures revealed in Figures 2 and 3 were indeed spherical, and they can be considered as extracellular vesicles. The spatial imaging of extracellular vesicles in the extracellular space of a TuMV-infected plant by FIB-EHR-SEM (Supplemental Movie S1) also suggested that these extracellular vesicles move within the cell wall.

TuMV Components Are Present in the Apoplastic Fluid of Infected Plants

We next collected the apoplastic fluid of *N. benthamiana* leaves infected with TuMV expressing 6K$_2$:GFP to confirm that viral components are present in the extracellular space. The collected fluid was ultracentrifuged to isolate the membrane fraction. An aliquot of the suspended membrane pellet was observed by confocal microscopy and showed green fluorescent punctae of the size expected for 6K$_2$:GFP (Fig. 5A). No fluorescent punctae was observed in apoplastic fluid collected from mock-infected plants, indicating that the observed signal is not the result of autofluorescence.

We also purified extracellular vesicles from infected Arabidopsis according to Rutter and Innes (2017). We first carried out apoplastic fluid extraction from Arabidopsis expressing PEN1-GFP, which is a marker for extracellular vesicles (Rutter and Innes, 2017). Green fluorescence punctae produced by PEN1-GFP were observed by confocal microscopy (Fig. 5B). To ensure that the detection of viral components was not the result of contaminating damaged cells, we also collected apoplastic fluid from Arabidopsis expressing the

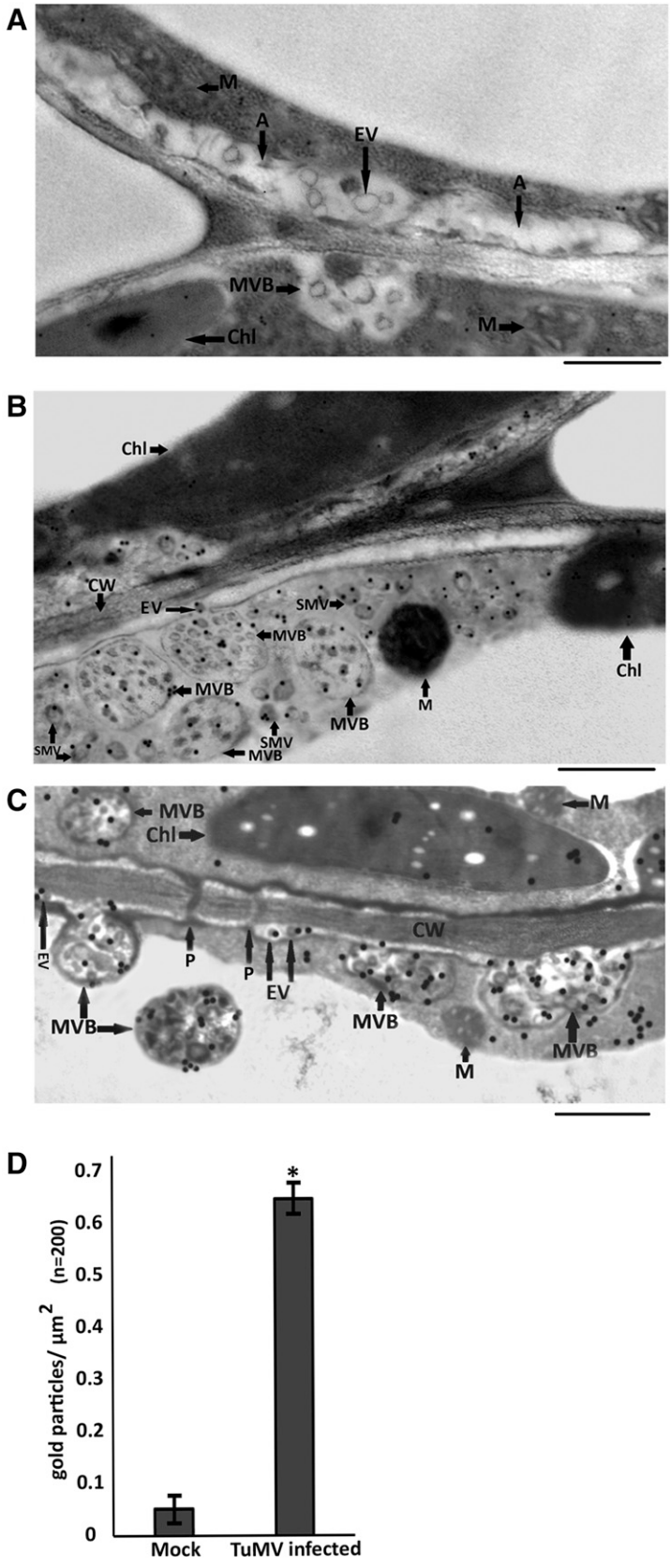

Figure 3. Extracellular vesicles and multivesicular bodies labeled with anti-dsRNA gold particles in TuMV-infected samples. Immunogold labeling was carried out on mock- and TuMV-infected *N. benthamiana* leaf sections by using an anti-dsRNA-specific antibody. A and B, TEM representative images showing gold labeling in (A) mock-infected condition and (B) TuMV-infected condition. C, Gold-labeled extracellular vesicles and MVBs fusing with the plasma membrane. Scale bars = 500 nm. D, Quantification of gold particles per μm^2 in mock- and TuMV-infected cells; each error bar = ±SD. Asterisk indicates significant difference is found (Student's *t* test, $n = 200$, P value < 0.05). EV, extracellular vesicle; A, apoplast; Chl, chloroplast; CW, cell wall; M, mitochondria; P, plasmodesmata; SMV, single-membrane vesicle.

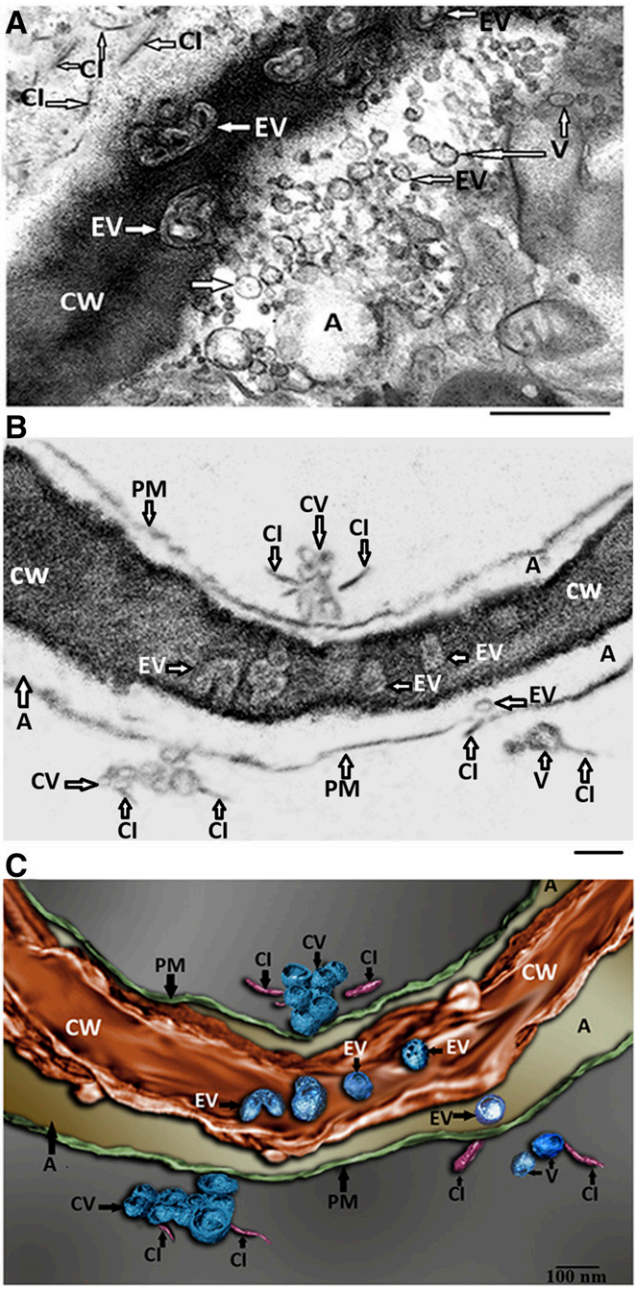

Figure 4. Three-dimension rendered image of extracellular vesicles in TuMV-infected sections. A, TEM image showing extracellular vesicles present within the cell wall of TuMV-infected cells. B, One image chosen from 350 images taken for FIB-EHRSEM. C, 3D rendered image showing vesicles in the extracellular space and the cell wall of TuMV-infected cells. A, apoplast; CI, cylindrical inclusion body; CW, cell wall; EV, extracellular vesicle; PM, plasma membrane; V, intracellular vesicle. Scale bar = 500 nm (A and 100 nm (B and C).

intracellular Golgi marker GmManI49-s yellow fluorescence protein (YFP; Rutter and Innes, 2017) and saw no YFP fluorescence (Fig. 5C). We also did not observe chloroplast autofluorescence emission in apoplastic fluid extracts, confirming that the extraction liquid was free of detectable cellular contamination.

Apoplastic fluid was then processed for extracellular vesicle purification. The collected membrane fraction was analyzed for the presence of $6K_2$:GFP by confocal microscopy. Green fluorescence punctae of an average diameter of 300 nm, as well as larger structures (~5–20 μm) likely resulting from clumped vesicles, were detected in extracts from infected plants (Fig. 5D). No green fluorescence was observed in mock-infected extracts. We then performed an immunoblot analysis with anti-GFP serum on purified extracellular vesicle extracts from mock- and TuMV/$6K_2$:GFP-infected plants (Fig. 5E). The analysis confirmed that the green fluorescent punctae observed by confocal microscopy is the consequence of the presence of $6K_2$:GFP in the apoplastic fluid. We noted that there was proteolytic degradation of $6K_2$:GFP in the apoplast fraction. This degradation is likely a result of proteolytic degradation that occurred in the extracellular space (Zheng et al., 2004). Total RNA was also extracted from purified extracellular vesicles and subjected to reverse transcription PCR (RT-PCR) using primers for $6K_2$-coding sequence amplification. A fragment of 162 bp, which is the expected size for the RT-PCR amplification of the $6K_2$-coding sequence, was detected only in infected plants (Fig. 5F). These data indicate that $6K_2$-tagged extracellular vesicles containing vRNA are produced during infection.

Proteomic Analysis Shows the Presence of Viral Proteins and Host Immune Response-Related Proteins in Extracellular-Vesicle–Enriched Fractions

To better characterize the content of $6K_2$-tagged extracellular vesicles and identify its associated proteins, we isolated them as described earlier, solubilized the membranes to release all associated proteins (peripheral, transmembranous, and internal), and carried out tandem mass spectrometry (MS/MS) proteomic analysis on extracellular vesicle-enriched fractions from mock- and TuMV-infected *N. benthamiana*. Because vRNA associates with multiple proteins to form a ribonucleoprotein complex, called a "viral replication complex" that is nested into viral factories, we bioinformatically analyzed the proteomes to primarily search for potential viral protein matches. Viral proteins were exclusively detected in TuMV-infected conditions but not in mock conditions. Peptides spanning the TuMV polyprotein were detected in the infected extracellular vesicle-enriched fractions, with the exception of $6K_1$ and $6K_2$ (Fig. 6; Supplemental Fig. S1). Nevertheless, the presence $6K_2$ can be inferred owing to the detection of GFP tryptic peptides in infectious conditions (Supplemental Table S1). Because no TuMV filamentous viral particles were observed by TEM in the extracellular space in the vicinity of TuMV-induced extracellular vesicles (Figs. 2–4) and the tryptic peptides from the proteomic analysis were not exclusively from the viral coat protein, but derived from the TuMV polyprotein (Fig. 6; Supplemental Fig. S1), it would

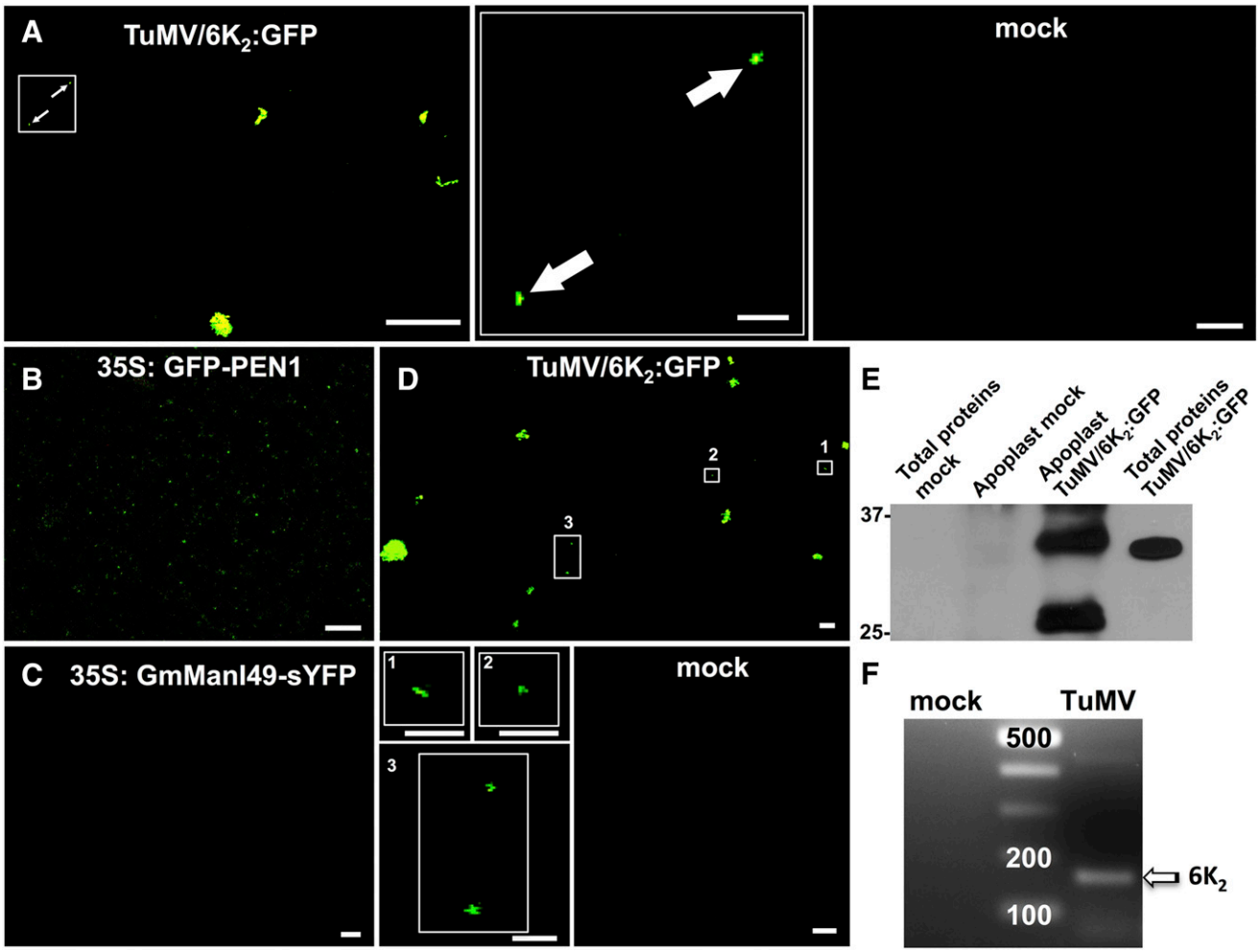

Figure 5. $6K_2$ isolated from apoplastic fluid during TuMV infection. A–D, Confocal microscopy performed on purified extracellular membrane fractions from (A) TuMV- (left and middle zoom in inset) and mock- (right) infected *N. benthamiana* leaves; (B) PEN1-GFP expressed Arabidopsis; (C) GmManI49-sYFP expressed Arabidopsis; (D) *Col-0 Arabidopsis* plants inoculated with pCambiaTuMV/$6K_2$:GFP (upper- and lower-left zoom for insets 1–3) or pCambia1380 (mock, lower right). E, Western-blot analysis with anti-GFP antibodies of extracellular-vesicle–purified fractions and total protein extractions from mock- and TuMV-infected *Arabidopsis Col-0* wild-type plants. F, Agarose gel electrophoresis of the RT-PCR performed on RNA from extracellular-vesicle–purified fractions from mock- and TuMV-infected conditions. Scale bars = 10 μm.

indicate that at least a subset of the extracellular vesicle fractions contains TuMV replication complexes. We also identified ~100 host proteins with a probability >95% and from at least two tryptic peptide matches when compared to the *N. benthamiana* proteome (Supplemental Table S1). Comparison of mock-infected and TuMV-infected sample proteomes through the Venn diagram representation revealed that 62% of the proteins were present in both conditions (Fig. 7A). Twenty-six host proteins were exclusively detected in infectious conditions. Poly-A binding protein (PABP) and heat shock protein Hsp70, previously characterized as being in TuMV replication factories to support viral replication (Léonard et al., 2004; Dufresne et al., 2008), were exclusively detected in extracts from TuMV-infected conditions (Supplemental Table S2), which supports the idea that the isolated extracellular vesicles likely contain TuMV replication complexes. In addition to PABP, other proteins of nuclear origin were also detected. Interestingly, in TuMV extracellular vesicle-enriched fractions, we found that some enzymes involved in lipid and secondary metabolite biosynthesis pathways were present (e.g. sesquiterpene synthase, 9-lipoxygenase; Supplemental Table S2). During host-pathogen interactions, plants secrete a plethora of proteases from diverse subcellular origins (cytosolic, nuclear, vacuolar) into the apoplastic space, but little is known about the means used for their release. For instance, cathepsin B was detected exclusively in TuMV-infected conditions. Cathepsin B is a cysteine protease secreted in the apoplast to counteract pathogens and regulate the hypersensitive response (Gilroy et al., 2007). We identified many proteins involved in plant defense and immunity, such as the plant pathogenesis-related

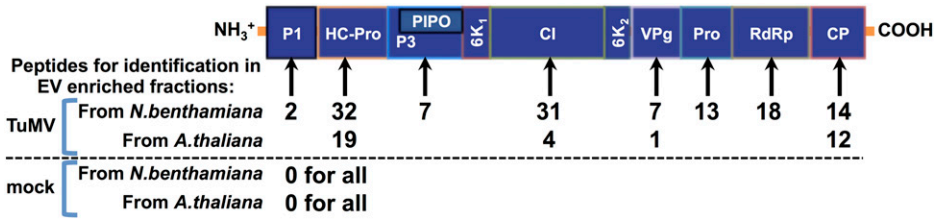

Figure 6. Distribution of tryptic peptides on TuMV polyprotein. TuMV polyprotein is depicted as a blue rectangle with individual fully processed proteins indicated. The number below the arrow indicates the number of peptides identified for a given protein in the proteome analysis of extracellular vesicle purified fractions of *N. benthamiana*. P1, Ser protease protein1; HC-Pro, Helper component proteinase; P3, protein3; PIPO, Pretty Interesting Potyviridae ORF (open reading frame); $6K_1$, 6kDa protein1; CI, cylindrical inclusion protein; $6K_2$, 6kDa protein2; VPg, genome-linked viral protein; Pro, Nuclear inclusion A protease Pro; RdRp, vRNA-dependent RNA polymerase; CP, coat protein.

protein 10, and proteins belonging to the silencing pathway such as the argonaute protein AGO2 (Supplemental Tables S1 and S2).

Because the total proteome of *N. benthamiana* is not fully characterized, we also performed a proteomic analysis on Arabidopsis TuMV-induced extracellular vesicle extracts to have a better idea of their content. It is generally acknowledged that almost all cells potentially produce extracellular vesicles in particular contexts, conditions, or stimuli. Importantly, different organisms or hosts, as well as cells from different organs from the same organism, likely produce diverse subpopulations of extracellular vesicles with different contents in terms of proteins and nucleic acids (Willms et al., 2016) that may display different functions. Similarly to what was observed in *N. benthamiana*, we also detected multiple viral protein peptides in Arabidopsis exclusively in TuMV-enriched extracellular fractions (Fig. 6; Supplemental Fig. S1). In addition to TuMV proteins, we identified ~400 host proteins from at least two tryptic peptide matches when compared to the entire Arabidopsis proteome and a probability of identification >95% (Supplemental Tables S3 and S4). Comparison of mock-infected and TuMV-infected sample proteomes through the Venn diagram representation revealed that 72% of the proteins were present in both conditions (Fig. 7B). We also noticed the presence of host proteins (e.g. eEF1A) known to be associated with proteins belonging to TuMV replication vesicles, such as Hsp70-3 (Dufresne et al., 2008; Thivierge et al., 2008). We also detected the presence of other transcription factors in TuMV-induced extracellular vesicles such as eIF3, which may play a role during infection. We also detected multiple proteins involved in vesicle trafficking, for instance the exocyst protein Exo70-A1. Exocyst proteins are long tethering factors involved in membrane remodeling and are likely involved in extracellular vesicle production (Chacon-Heszele et al., 2014; Goring, 2017).

To better understand the potential biological function of the proteins identified in the extracellular vesicle fractions, we processed the proteomic data for gene ontology (GO) classification. Protein classification was made for the extracellular vesicle proteome from noninfected and infected conditions both for *N. benthamiana* and Arabidopsis in terms of different categories of biological processes through The Arabidopsis Information Resource (www.arabidopsis.org) using the "GO Term Enrichment for Plants" bioinformatics tool (Fig. 7, C and D). The bioinformatic analysis provides results in terms of percentages of the total proteome for each category. Detected proteins harbor different functions where some may have a supportive action for viral replication (e.g. PABP) whereas some others may display an antiviral effect (e.g. AGO2). Interestingly, comparison of the GO category distribution between mock- and TuMV-infected proteomes highlighted that host factors involved in the response to abiotic/biotic stresses, in interorganelle vesicular exchanges, as well as in regulation of translation processes were more represented in infectious conditions.

DISCUSSION

We report in this study that TuMV proteins and RNA are released in the extracellular space of infected plants as replication complexes within extracellular vesicles. This investigation and that of Wan et al. (2015) may thus change our way of looking at how viruses may spread within a plant.

Replication complexes of TuMV are initially assembled within endoplasmic-reticulum–derived $6K_2$-tagged vesicles (Grangeon et al., 2012; Jiang et al., 2015). These $6K_2$ replication vesicles are motile and move from one cell to another (Cotton et al., 2009; Grangeon et al., 2013). Here, we observed $6K_2$ as aggregates in the extracellular space of infected leaves (Fig. 1). $6K_2$ was also observed as similar aggregates in xylem-conducting tubes and were shown to consist of an amalgamation of vesicles containing vRNA and the viral RdRp (Wan et al., 2015). Because the extracellular space is connected to the xylem (Ligat et al., 2011), it reasonable to think that the $6K_2$ aggregates found in the extracellular space and the xylem are related. Therefore, what is observed in the intercellular space in the form of $6K_2$ aggregates would likely be membrane-associated viral replication complexes.

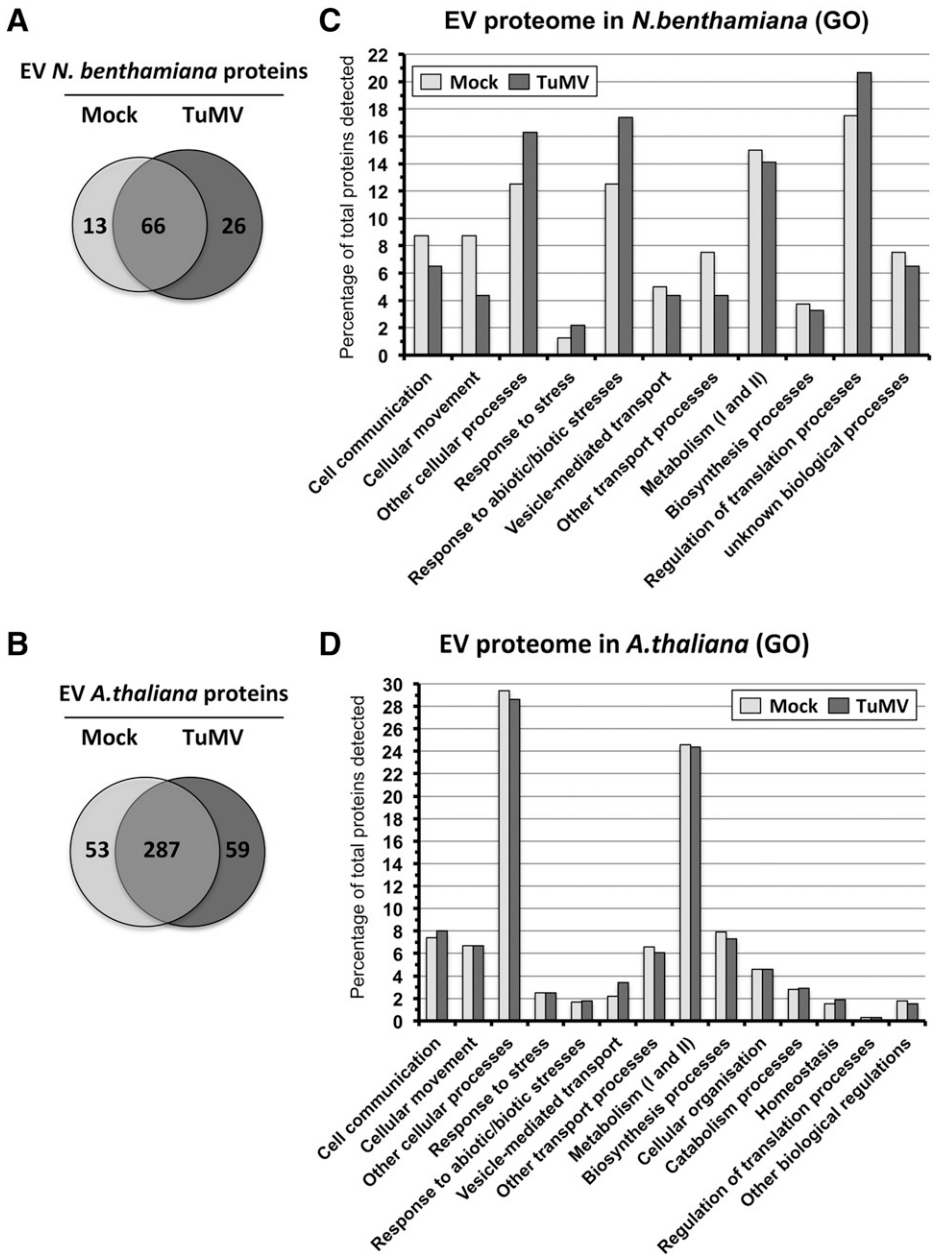

Figure 7. Proteomic analysis of purified extracellular vesicles. A and B, Venn diagram of protein distribution from the extracellular vesicle proteome from mock-inoculated and TuMV/$6K_2$:GFP-inoculated *N. benthamiana* plants (A) and *Arabidopsis Col-0* wild-type plants (B) based on their presence or absence in each condition. EV, extracellular vesicle. C, GO classification by biological processes of purified extracellular vesicle proteome from mock- and TuMV/$6K_2$:GFP-inoculated *N. benthamiana* plants. D, GO classification by biological processes of purified extracellular vesicle proteome from mock and TuMV/$6K_2$:GFP-inoculated Arabidopsis plants.

This assertion is supported by the observation of Cabanillas et al. (2018) that replication complexes of TuMV after their initial assembly into endoplasmic-reticulum–derived vesicles bypass the Golgi apparatus and that a subset of those replication vesicles ends up in MVBs. MVBs proliferate and fuse with the plasma membrane for the release of their intraluminal vesicles in the extracellular space after fungal and bacterial attack (An et al., 2006a, 2006b; Wang et al., 2014; Cai et al., 2018). Similarly, we observed in TuMV-infected samples that MVBs containing vRNA fused with the plasma membrane and released their vesicular content in the extracellular space (Figs. 2 and 3). The absence of $6K_2$:GFP and FM4-64 signal overlap (Fig. 1) further supports the idea that the presence of $6K_2$ in the extracellular space results from the release of intraluminal vesicles after fusion of MVBs with the plasma membrane. It is the outer membrane of MVBs that fuses with the plasma membrane. $6K_2$, being associated with intraluminal vesicles within MVBs, does not come into direct contact with the plasma membrane and are thus not stained by FM4-64. Proliferation of extracellular vesicles was also reported for plants infected by *Barley stripe mosaic virus* (McMullen et al., 1977).

The idea that plant extracellular vesicles could be involved in any plant biological processes has been challenged because of the presence of the cell wall, which should presumably prevent vesicles from passing through it. One argument given against this conception is the capacity of isolating vesicles from

apoplastic fluid (Rutter and Innes, 2017). In support of this argument, we observed that vesicles penetrated the cell wall (Fig. 4) and proteomic data revealed the presence of cell-wall–modifying proteins such as pectin acetylesterase (Supplemental Table S3). As lipid structures, it is possible that extracellular vesicles contain different subsets of lipids that confer special membrane fluidity properties and can compress as they move through pores in the cell wall. This may explain the distorted shape of some of the extracellular vesicles within the cell wall.

The association of TuMV components in extracellular vesicles was also confirmed by biochemical means both in *N. benthamiana* and Arabidopsis (Fig. 5). Furthermore, proteomic data indicated that the viral peptides spanned the whole TuMV polyprotein (Fig. 6; Supplemental Fig. S1). Host proteins associated with TuMV replication proteins were also detected in the extracellular vesicle extracts from infected material (e.g. PABP; Supplemental Tables S1–S4), which supports the idea that extracellular vesicles contain TuMV replication factories.

Host proteins involved in RNA silencing were detected in extracellular vesicle extracts (Fig. 7; Supplemental Tables S1 and S2), which might or might not be associated with the TuMV extracellular vesicles. Of particular interest, we found proteins involved in plant response to viral infection, such as s-adenosylhomo-Cys hydrolase (Cañizares et al., 2013; Lionetti et al., 2014a, 2014b) and AGO2, which is involved in TuMV infection (Garcia-Ruiz et al., 2015). We also identified the 14-3-3 protein that has a role in plant signal transduction and immunity response and can be induced during *Tobacco mosaic virus* infection (Wang et al., 2016). Furthermore, proteins essential for endomembrane remodeling and interorganelle vesicular exchanges were detected. For example, synaptotagmin A, known to be important for endoplasmic reticulum–plasma membrane contacts and vesicle trafficking, was found at similar levels in mock- and TuMV-infected extracellular-enriched fractions and may have an important role in extracellular vesicle tethering. Furthermore, synaptotagmin A was found to be important for TuMV infection (Uchiyama et al., 2014) and might have a role in TuMV-induced–extracellular vesicle trafficking. Also, Rab proteins, such as RabG3E, RabD2B, and Rab7, as well as the SNARE proteins SYP71, SYP132, and SYP121, the exocyst EXO70-A1, and COP I coatomer protein were detected and may display an important role once the extracellular vesicles reach their destination for membrane interaction. Several ATPases, including the vesicle-fusing ATPase protein, were detected and are likely required for providing the energy for the membrane fusion events. A semiquantitative comparison of peptide abundance based on exclusive peptide spectrum counts for individual proteins suggested that some proteins are preferentially found in extracellular vesicles from TuMV-infected plants. For instance, we found that some enzymes, such as glyceraldehyde-3-P dehydrogenase and lipoxygenases, were present in the TuMV extracellular vesicle fraction proteome. In addition to its role in primary metabolism, the presence of glyceraldehyde-3-P dehydrogenase in viral factories and its importance during viral replication was previously shown for Tomato Bushy Stunt Virus (Wang and Nagy, 2008). Also, the presence of lipoxygenases (e.g. 9-lipoxygenase) in TuMV-extracellular–enriched fractions may have an important role in the viral replication complex. For instance, a lipoxygenase was found to interact with the eIF4E transcription factor and eIF4E is known to be crucial for *Potyvirus* replication (Freire et al., 2000). Furthermore, we identified a tetraspanin protein seemingly more present in TuMV-extracellular–enriched fractions. Also, increasing evidence on animal and plant extracellular vesicles are pointing out that tetraspanin transmembrane proteins could be a hallmark of at least a subset of extracellular vesicles produced in different contexts (Perez-Hernandez et al., 2013; Guix et al., 2017; Cai et al., 2018). We also found translation factors seemingly present more often in infected extracts, such as eIF5A and eIF3, which have been associated with viral infections (Bureau et al., 2004; Ryabova et al., 2004; Chen et al., 2017). Interestingly, extracellular vesicles across kingdoms carry a variety of proteins with multiple functions and intracellular origin, nevertheless some turned out to be associated with extracellular vesicles. For instance, some nuclear proteins were found to be associated with animal exosomes such as the RNA-binding protein Y-box protein1 (Buschow et al., 2010; Shurtleff et al., 2016). In this study, we found that some transcription factors and nuclear GTPases (e.g. Ran) where present in TuMV infectious conditions. Some molecular channels regulating membrane permeability, such as aquaporins (e.g. PIP1,2 and TIP2,1), were likely more present in TuMV-infectious conditions (Supplemental Table S3). Recent evidence indicates that aquaporins from different subcellular origin associate with extracellular vesicles and could potentially be used as markers for diagnostic assays (Pegtel et al., 2014). Also, it is known that some aquaporins interact with SNARE proteins for their trafficking, including SYP121 (Hachez et al., 2014), and notably, SYP121 was present exclusively in TuMV-enriched extracellular vesicles. Finally, we compared our total proteome to the extracellular vesicle proteome characterized by Rutter and Innes (2017). In addition to PEN1, we found that ~41% of the proteins, including vacuolar proteins, were in common for both proteomes. This suggests that some proteins might form part of a general mechanism whereby certain proteins are recruited to extracellular vesicles for a broad range of pathogen infections.

These findings not only support the idea that extracellular $6K_2$-tagged vesicles contain TuMV replication complexes, but also suggest that a plant defense response is possibly taking place against TuMV in the extracellular space. Pathogen perception by the plant innate immune system is mediated by microbe/danger-associated molecular patterns (MAMPs/DAMPs) that are recognized by pattern recognition receptors (PRRs) on the plasma membrane (Macho and Zipfel, 2014). Ligand binding to

PRRs for nonviral pathogens takes place on the apoplastic side of the membrane. Although the recognition of MAMPs/DAMPs is believed to occur intracellularly in the case of viruses (Ding and Voinnet, 2007), a recent study reported on the possible involvement of plasma membrane-localized receptor-like kinases in MAMP recognition by PRRs in plant-virus interactions (Kørner et al., 2013). Thus, it will be interesting to see if any of the components of TuMV could act as extracellular MAMPs/DAMPs.

It is also possible that viral infection can spread systemically through extracellular replication vesicles. Stem girdling experiments showed that TuMV infection can proceed from xylem vessels and that xylem sap is infectious (Wan and Laliberté, 2015). However, isolating a large volume of apoplastic fluid devoid of cellular debris, in addition to the instability of purified extracellular vesicles, will be a challenging task for demonstrating if vRNA-containing extracellular vesicles are indeed infectious.

MATERIALS AND METHODS

Plant Materials

The leaves of 6- to 8-week–old *Nicotiana benthamiana* plants were used for transient expression analyses and virus inoculations. *N. benthamiana* seeds were grown directly on soil at 20°C to 22°C under constant light. Wild-type Arabidopsis (*Arabidopsis thaliana*) plants were ecotype *Col-0*. Transgenic plant lines were of the *Col-0* background and were obtained from Roger Innes's laboratory: 35S::GFP-PEN1 (Meyer et al., 2009) and 35S::GmMANI49-sYFP transgenic lines (Gu and Innes, 2012). Seeds were stratified for 2 d at 4°C and plants were grown at 22°C with a photoperiod of 16-h light and 8-h dark.

Agrobacterium Infiltration of *N. benthamiana*

pCambiaTuMV/6K$_2$:GFP was transformed into *Agrobacterium tumefaciens* by electroporation. *A. tumefaciens* containing the plasmid was grown in Lysogeny broth supplemented with kanamycin overnight at 28°C with shaking. The cells were centrifuged at 2000*g* for 10 min and resuspended in infiltration buffer (10 mM of $MgCl_2$ and 150 μM of acetosyringone). The cell suspension was incubated for 4 h at room temperature before infiltration. The OD_{600} was adjusted to 0.40 for infiltration.

Confocal Microscopy

Agroinfiltrated leaf sections were imaged using a model no. SP8 with the 63× immersion objective (Leica). A laser of 488 nm was used to excite GFP and the capture was done at 500–540 nm. For FM4-64, the excitation/emission maxima were 543/640 nm. Image processing to reconstruct a 3D image was done using the image analysis software Imaris (Bitplane). For detection of GFP fluorescence from purified extracellular vesicles, a small volume of resuspended pellets was observed using a model no. LSM780 Inverted Confocal Microscope with a 63× oil immersion objective (Zeiss). GFP and YFP chromophores were excited at 488 nm, and the emission light was acquired from 495-nm to 550-nm wavelengths. Chloroplast autofluorescence was acquired from 630 nm to 680 nm. Plasma membrane staining with FM4-64 was done as follows: *N. benthamiana* leaves were cut at 6 dpi and dipped in 1 μg/μL of FM4-64 (N-[3-triethylammoniumpropyl]-4-[6-(4-[diethylamino]phenyl)hexatrienyl]-pyridinium dibromide) dye. Leaves were incubated at room temperature for 30 min and observed by confocal laser microscopy.

TEM

Small pieces (1.5 × 2 mm) of TuMV systemically infected (upper-non-infiltrated) leaves of *N. benthamiana* were cut and fixed in 2.5% (w/v) glutaraldehyde in 0.1 M of sodium cacodylate buffer, at pH 7.4, for 24 h at 4°C as described in Movahed et al. (2017). The sections were examined in a Tecnai T12 Transmission Electron Microscope (FEI) operating at 120 kV. Images were recorded using an AMT XR80C charge-coupled-device camera system (FEI). The number of various TuMV replication vesicles during systemic infection was counted manually from the TEM images. For immuno-gold labeling, large pieces (1.5 × 5 mm) of mock- and TuMV-infected leaves of *N. benthamiana* were cut at 6 dpi and fixed in 4% (w/v) formaldehyde and 0.25% (w/v) glutaraldehyde in 0.1-M Sorensen's phosphate buffer, pH 7.4, for 4 h at 4°C. After rinsing the samples three times for 10 min each in washing buffer at room temperature, samples were postfixed in 0.1% (w/v) reduced osmium tetroxide for 15 min at 4°C (Kopek et al., 2007). The samples were then rinsed in water at room temperature (three times for 10 min each) and dehydrated in a graded alcohol series (30%, 50%, 70%, 80%, 90%, 95%, and 100%, v/v) for 20 min at each step at 4°C on a rotator. Rinsing in 100% alcohol was repeated one more time. The samples were then gradually infiltrated with increasing concentrations of London Resin white resin (50%, 75% ,and 100%, v/v) mixed with acetone for a minimum of 8 h for each step at 4°C on a rotator. The samples were finally embedded in pure London Resin white resin and polymerized at 50°C for 48 h. Next, 90–100-nm sections were incubated in 20-mM Gly in Dulbecco's phosphate-buffered saline (DPBS [137 mM of NaCl, 2.7 mM of KCl, 1.5 mM of KH_2PO_4, 6.5 of mM Na_2HPO_4, 1 mM of $CaCl_2$, 0.5 mM of $MgCl_2$, at pH 7.4]) for 10 min to inactivate residual aldehyde groups, and then in blocking solution (DPBS-BCO: 2% [w/v] bovine serum albumin, 2% [w/v] casein, and 0.5% [w/v] ovalbumin in DPBS) for 5 min. Sections were then incubated with the mouse monoclonal anti-dsRNA antibody J2 (stock solution is 1 mg/mL; English and Scientific Consulting Kft./SCICONS) diluted in DPBS-BCO (1:20) for 1 h at room temperature. After six washings (5 min each) in DPBS and 5 min in blocking buffer, sections were incubated with the goat anti-mouse secondary antibody, conjugated to 10-nm gold particles (Sigma-Aldrich), diluted in DPBS-BCO 1:20. After washing with DPBS and distilled water, grids were stained with 4% (w/v) uranyl acetate for 2 min and Reynolds lead citrate for 2 min. Background labeling was determined using mock-infected leaf cross sections. Quantification of the distribution of the gold particles per μm^2 and relative labeling distribution were performed over mock-infected and TuMV-infected sections according to Lucocq et al. (2004). Two different labeling experiments were considered, and 20 different cells were studied for each treatment and 200 gold particles were counted per experiment.

FIB–SEM

The sample block for the FIB-SEM was prepared using the same protocol as TEM processing. The trimmed Epon block of TuMV-infected leaf was mounted on a 45° pretitled SEM stub and then coated with 4 nm of Pt to enhance electrical conductivity. The principle of imaging is based on using a FIB to create a cut at a designated site in the specimen (TuMV-infected cell), followed by viewing the newly generated surface with a scanning electron beam. Iteration of these two steps 350 times resulted in the generation of a series of surface maps of the plant cell at regularly spaced intervals, which was converted into a 3D map. The experiment was performed using a dual-beam FIB (Helios Nanolab 660; FEI) equipped with a gallium ion source. A rectangular section (2-μm thick) of a Pt protection layer was deposited on the top of the surface of the area of interest to protect the resin volume and correct for stage and/or specimen drift; i.e. perpendicular to the image face, of the volume to be milled. Trenches on each side have been created to minimize the redeposition during slice and view. Distinct imaging fiducials were generated for both ion beam and electron beam imaging and were used to dynamically correct for any drift in x and y during a run by applying appropriate SEM beam shifts. Slicing was obtained at 30 kV with an ion beam current of 2.5 nA at a stage 6.5° tilt and working distance of 4 mm. With each step, 7 nm of the material was removed with the ion beam and the newly occurring block face was imaged with the electron beam at an accelerating voltage of 2 kV and beam current of 0.4 nA using the backscattered electron signal recorded with a through-the-lens detector at a stage tilt of 41.5° and working distance of 3 mm. The pixel size was 8 nm with a dwell time of 30 μs and pixel dimensions of the recorded image were 1,536 × 1,024 pixels. This process was collected using the software module Auto Slice and View G3 1.5.3 from FEI. Finally, 350 back-scattered images were collected, and the contrast of the images was inversed. The imaging parameters were set to optimize for best signal-to-noise ratios and resolution in images. Image stacks were aligned and reconstructed using Amira 6.0 (FEI). The Volren module from Amira was applied for direct 3D visualization. Snapshots and movies were generated on various areas of interest.

Extracellular Vesicle Purification

Plants were grown for 5–6 weeks and inoculated with *A. tumefaciens* containing either the pCambia 1380 vector for mock conditions or the infectious clone pCambiaTuMV/6K$_2$:GFP before being harvested at 15 dpi. The *Agrobacterium* suspension was adjusted to an OD$_{600}$ of 0.015. Vesicles were isolated from rosettes and the apoplastic wash was performed with vesicle isolation buffer (VIB) solution as described in Rutter and Innes (2017). Briefly, infiltrated plants were centrifuged at 700*g* for 20 min at 4°C. The apoplastic wash was filtered through a 0.45-μm membrane and centrifuged at 10,000*g* for 30 min and ultracentrifuged at 100,000*g* for 60 min at 2°C. The obtained pellet was resuspended in VIB solution for further analyses by MS, western blot, or RNA extraction. Western-blot analysis was performed as described in Jiang et al. (2015).

RNA Extraction and RT-PCR

The extracellular vesicle-isolated pellets from mock- and TuMV-infectious conditions were washed twice in VIB buffer by ultracentrifugation at 100,000*g* for 60 min at 2°C. Total RNA extraction was performed on the extracellular vesicle-isolated pellet with phenol/chloroform/isoamyl alcohol (UltraPure 15593031; Invitrogen). Phenol/chloroform/isoamyl alcohol was mixed to the resuspended pellet at a 1:1 (v/v) ratio, respectively, and centrifuged for 15 min, 16,000*g* at 4°C. The resulting aqueous phase was mixed with sodium acetate and anhydrous ethanol, at a 20:1:2.5 ratio (v/v), respectively, and was kept at −20°C for 3 h and then centrifuged for 1 h, 16,000*g* at 4°C. The obtained pellet was resuspended in ethanol 70%, centrifuged, and dried before its final solubilization in Ultrapure RNAse-free water. Reverse transcription was performed with the iScript cDNA Synthesis Kit (Bio-Rad). PCR was performed on the resulting cDNAs with specific primers targeting the 6K$_2$ viral protein encoding sequence (forward sequence: 5′-CACCATGAACACCAGCGACATGAGC-3′; reverse sequence: TTCATGGGTTACGGGTTCGGACATC-3′).

MS

Extracellular vesicles were isolated from Arabidopsis *Col-0* inoculated with pCambiaTuMV/6K$_2$:GFP or pCambia1380. Membranes were solubilized, and proteins denatured with the Protease Max thermosensitive surfactant (Promega). Solubilized samples were processed for trypsin digestion and liquid chromatography-coupled to MS/MS, similarly as described in Cloutier et al. (2014). All MS/MS samples were analyzed using the software Mascot (v2.5.1; Matrix Science). Mascot was set up to search the NCBI_Arabidopsis_Thaliana_txid3702 database (unknown version, 73,710 entries) assuming the digestion enzyme trypsin. Mascot was searched with a fragment ion mass tolerance of 0.60 D and a parent ion tolerance of 10.0 μL^{-1}. O+18 of pyrro-Lys and carbamidomethyl of Cys were specified in Mascot as fixed modifications. Oxidation of Met was specified in Mascot as a variable modification. Scaffold software (Proteome Software) was used to validate MS/MS-based peptide and protein identifications. Peptide identifications were accepted if they exceeded specific database search engine thresholds. Mascot identifications required that at least ion scores must be greater than both the associated identity scores and 30, 30, 25, and 25 for singly, doubly, triply, and quadrupally charged peptides. Protein identifications were accepted if they contained at least two identified peptides (except for PEN1, where one-peptide–match identification was considered). Proteins that contained similar peptides and could not be differentiated based on MS/MS analysis alone were grouped to satisfy the principles of parsimony. Only proteins identified with a probability >95% were considered for further analyses. All proteome analyses were further processed for GO categorization in terms of biological processes by using the "GO Term Enrichment for Plants" bioinformatics tool available on The Arabidopsis Information Resource website (www.arabidopsis.org).

Accession Numbers

Sequence data from this article can be found in the GenBank database under the following accession numbers for TuMV 1494058 for *N. benthamiana*: gi|400234898; gi|48716124; gi|594551320; gi|505490393; gi|94958151, gi|661761869, gi|332649837; gi|387861274; gi|115315688; and for Arabidopsis: gi|145323788; gi|15228840, gi|22326587, gi|18415308; gi|12230867; gi|1345592; gi|330252015; gi|332194293; gi|18422766; gi|332192158; gi|28380165; gi|18415701; gi|332195054; gi|28380149; gi|186528371; gi|332190895; gi|332644528; gi|145324016; gi|1175011; gi|32363275; gi|28380149. Accession numbers for other genes are reported in the Supplemental Tables S1–S4.

Supplemental Data

The following supplemental materials are available.

Supplemental Figure S1. Tryptic peptide sequences aligned on the TuMV polyprotein sequence.

Supplemental Movie S1. Spatial imaging of extracellular vesicles in the extracellular space of a TuMV-infected plant by FIB-EHRSEM.

Supplemental Table S1. Proteome of purified extracellular vesicles from mock- and TuMV-infected *N. benthamiana*.

Supplemental Table S2. Proteome of purified extracellular vesicles exclusive to TuMV-infected conditions in *N. benthamiana*.

Supplemental Table S3. Proteome of purified extracellular vesicles from mock- and TuMV-infected Arabidopsis.

Supplemental Table S4. Proteome of purified extracellular vesicles exclusive to TuMV-infected conditions in Arabidopsis.

ACKNOWLEDGMENTS

We thank the research group of the Facility for Electron Microscopy Research at McGill University, where we conducted all the experiments of TEM and FIB Systems and Dual Beam microscopy. We thank Roger Innes (Indiana State University) for providing 35S::GFP-PEN1 and 35S::GmMANI49-sYFP transgenic plants.

Received March 27, 2019; accepted April 11, 2019; published April 24, 2019.

LITERATURE CITED

Abels ER, Breakefield XO (2016) Introduction to extracellular vesicles: Biogenesis, RNA cargo selection, content, release, and uptake. Cell Mol Neurobiol **36:** 301–312

Agbeci M, Grangeon R, Nelson RS, Zheng H, Laliberté JF (2013) Contribution of host intracellular transport machineries to intercellular movement of turnip mosaic virus. PLoS Pathog **9:** e1003683

Ahsan NA, Sampey GC, Lepene B, Akpamagbo Y, Barclay RA, Iordanskiy S, Hakami RM, Kashanchi F (2016) Presence of viral RNA and proteins in exosomes from cellular clones resistant to Rift Valley Fever virus infection. Front Microbiol **7:** 139

Akers JC, Gonda D, Kim R, Carter BS, Chen CC (2013) Biogenesis of extracellular vesicles (EV): Exosomes, microvesicles, retrovirus-like vesicles, and apoptotic bodies. J Neurooncol **113:** 1–11

An Q, Ehlers K, Kogel KH, van Bel AJ, Hückelhoven R (2006a) Multivesicular compartments proliferate in susceptible and resistant MLA12-barley leaves in response to infection by the biotrophic powdery mildew fungus. New Phytol **172:** 563–576

An Q, Hückelhoven R, Kogel KH, van Bel AJ (2006b) Multivesicular bodies participate in a cell wall-associated defence response in barley leaves attacked by the pathogenic powdery mildew fungus. Cell Microbiol **8:** 1009–1019

Arenaccio C, Chiozzini C, Columba-Cabezas S, Manfredi F, Affabris E, Baur A, Federico M (2014) Exosomes from human immunodeficiency virus type 1 (HIV-1)-infected cells license quiescent CD^{4+} T lymphocytes to replicate HIV-1 through a Nef- and ADAM17-dependent mechanism. J Virol **88:** 11529–11539

Baldrich P, Rutter BD, Karimi HZ, Podicheti R, Meyers BC, Innes RW (2019) Plant extracellular vesicles contain diverse small RNA species and are enriched in 10- to 17-nucleotide "tiny" RNAs. Plant Cell **31:** 315–324

Bern MM (2017) Extracellular vesicles: How they interact with endothelium, potentially contributing to metastatic cancer cell implants. Clin Transl Med **6:** 33

Bukong TN, Momen-Heravi F, Kodys K, Bala S, Szabo G (2014) Exosomes from hepatitis C infected patients transmit HCV infection and contain replication competent viral RNA in complex with Ago2-miR122-HSP90. PLoS Pathog **10:** e1004424

Bureau M, Leh V, Haas M, Geldreich A, Ryabova L, Yot P, Keller M (2004) P6 protein of Cauliflower mosaic virus, a translation reinitiator, interacts with ribosomal protein L13 from *Arabidopsis thaliana*. J Gen Virol **85:** 3765–3775

Buschow SI, van Balkom BW, Aalberts M, Heck AJ, Wauben M, Stoorvogel W (2010) MHC class II-associated proteins in B-cell exosomes and potential functional implications for exosome biogenesis. Immunol Cell Biol **88:** 851–856

Cabanillas DG, Jiang J, Movahed N, Germain H, Yamaji Y, Zheng H, Laliberté JF (2018) Turnip mosaic virus uses the SNARE protein VTI11 in an unconventional route for replication vesicle trafficking. Plant Cell **30:** 2594–2615

Cai Q, Qiao L, Wang M, He B, Lin FM, Palmquist J, Huang SD, Jin H (2018) Plants send small RNAs in extracellular vesicles to fungal pathogen to silence virulence genes. Science **360:** 1126–1129

Canitano A, Venturi G, Borghi M, Ammendolia MG, Fais S (2013) Exosomes released in vitro from Epstein-Barr virus (EBV)-infected cells contain EBV-encoded latent phase mRNAs. Cancer Lett **337:** 193–199

Cañizares MC, Lozano-Durán R, Canto T, Bejarano ER, Bisaro DM, Navas-Castillo J, Moriones E (2013) Effects of the crinivirus coat protein-interacting plant protein SAHH on post-transcriptional RNA silencing and its suppression. Mol Plant Microbe Interact **26:** 1004–1015

Chacon-Heszele MF, Choi SY, Zuo X, Baek JI, Ward C, Lipschutz JH (2014) The exocyst and regulatory GTPases in urinary exosomes. Physiol Rep **2:** e12116

Chen H, Adam Arsovski A, Yu K, Wang A (2017) Deep sequencing leads to the identification of eukaryotic translation initiation factor 5A as a key element in Rsv1-mediated lethal systemic hypersensitive response to soybean mosaic virus infection in soybean. Mol Plant Pathol **18:** 391–404

Ciregia F, Urbani A, Palmisano G (2017) Extracellular vesicles in brain tumors and neurodegenerative diseases. Front Mol Neurosci **10:** 276

Cloutier P, Lavallée-Adam M, Faubert D, Blanchette M, Coulombe B (2014) Methylation of the DNA/RNA-binding protein Kin17 by METTL22 affects its association with chromatin. J Proteomics **100:** 115–124

Cotton S, Grangeon R, Thivierge K, Mathieu I, Ide C, Wei T, Wang A, Laliberté J-F (2009) Turnip mosaic virus RNA replication complex vesicles are mobile, align with microfilaments, and are each derived from a single viral genome. J Virol **83:** 10460–10471

Ding SW, Voinnet O (2007) Antiviral immunity directed by small RNAs. Cell **130:** 413–426

Dreyer F, Baur A (2016) Biogenesis and functions of exosomes and extracellular vesicles. Methods Mol Biol **1448:** 201–216

Dufresne PJ, Thivierge K, Cotton S, Beauchemin C, Ide C, Ubalijoro E, Laliberté JF, Fortin MG (2008) Heat shock 70 protein interaction with turnip mosaic virus RNA-dependent RNA polymerase within virus-induced membrane vesicles. Virology **374:** 217–227

Feng Z, Hensley L, McKnight KL, Hu F, Madden V, Ping L, Jeong SH, Walker C, Lanford RE, Lemon SM (2013) A pathogenic picornavirus acquires an envelope by hijacking cellular membranes. Nature **496:** 367–371

Fleshner M, Crane CR (2017) Exosomes, DAMPs and miRNA: Features of stress physiology and immune homeostasis. Trends Immunol **38:** 768–776

Freire MA, Tourneur C, Granier F, Camonis J, El Amrani A, Browning KS, Robaglia C (2000) Plant lipoxygenase 2 is a translation initiation factor-4E-binding protein. Plant Mol Biol **44:** 129–140

Garcia-Ruiz H, Carbonell A, Hoyer JS, Fahlgren N, Gilbert KB, Takeda A, Giampetruzzi A, Garcia Ruiz MT, McGinn MG, Lowery N, et al (2015) Roles and programming of Arabidopsis ARGONAUTE proteins during turnip mosaic virus infection. PLoS Pathog **11:** e1004755

Gilroy EM, Hein I, van der Hoorn R, Boevink PC, Venter E, McLellan H, Kaffarnik F, Hrubikova K, Shaw J, Holeva M, et al (2007) Involvement of cathepsin B in the plant disease resistance hypersensitive response. Plant J **52:** 1–13

Goring DR (2017) Exocyst, exosomes, and autophagy in the regulation of Brassicaceae pollen-stigma interactions. J Exp Bot **69:** 69–78

Grangeon R, Agbeci M, Chen J, Grondin G, Zheng H, Laliberté JF (2012) Impact on the endoplasmic reticulum and Golgi apparatus of turnip mosaic virus infection. J Virol **86:** 9255–9265

Grangeon R, Jiang J, Wan J, Agbeci M, Zheng H, Laliberté JF (2013) 6K2-induced vesicles can move cell to cell during turnip mosaic virus infection. Front Microbiol **4:** 351

Gu Y, Innes RW (2012) The KEEP ON GOING protein of Arabidopsis regulates intracellular protein trafficking and is degraded during fungal infection. Plant Cell **24:** 4717–4730

Guix FX, Sannerud R, Berditchevski F, Arranz AM, Horré K, Snellinx A, Thathiah A, Saido T, Saito T, Rajesh S, et al (2017) Tetraspanin 6: A pivotal protein of the multiple vesicular body determining exosome release and lysosomal degradation of amyloid precursor protein fragments. Mol Neurodegener **12:** 25

György B, Szabó TG, Pásztói M, Pál Z, Misják P, Aradi B, László V, Pállinger E, Pap E, Kittel A, et al (2011) Membrane vesicles, current state-of-the-art: Emerging role of extracellular vesicles. Cell Mol Life Sci **68:** 2667–2688

Hachez C, Veljanovski V, Reinhardt H, Guillaumot D, Vanhee C, Chaumont F, Batoko H (2014) The Arabidopsis abiotic stress-induced TSPO-related protein reduces cell-surface expression of the aquaporin PIP2;7 through protein-protein interactions and autophagic degradation. Plant Cell **26:** 4974–4990

Jiang J, Patarroyo C, Garcia Cabanillas D, Zheng H, Laliberté JF (2015) The vesicle-forming 6K2 protein of turnip mosaic virus interacts with the COPII coatomer Sec24a for viral systemic infection. J Virol **89:** 6695–6710

Kopek BG, Perkins G, Miller DJ, Ellisman MH, Ahlquist P (2007) Three-dimensional analysis of a viral RNA replication complex reveals a virus-induced mini-organelle. PLoS Biol **5:** e220

Kørner CJ, Klauser D, Niehl A, Domínguez-Ferreras A, Chinchilla D, Boller T, Heinlein M, Hann DR (2013) The immunity regulator BAK1 contributes to resistance against diverse RNA viruses. Mol Plant Microbe Interact **26:** 1271–1280

Kouwaki T, Fukushima Y, Daito T, Sanada T, Yamamoto N, Mifsud EJ, Leong CR, Tsukiyama-Kohara K, Kohara M, Matsumoto M, et al (2016) Extracellular vesicles including exosomes regulate innate immune responses to hepatitis B virus infection. Front Immunol **7:** 335

Laliberté JF, Zheng H (2014) Viral manipulation of plant host membranes. Annu Rev Virol **1:** 237–259

Lawson C, Kovacs D, Finding E, Ulfelder E, Luis-Fuentes V (2017) Extracellular vesicles: Evolutionarily conserved mediators of intercellular communication. Yale J Biol Med **90:** 481–491

Léonard S, Viel C, Beauchemin C, Daigneault N, Fortin MG, Laliberté JF (2004) Interaction of VPg-Pro of turnip mosaic virus with the translation initiation factor 4E and the poly(A)-binding protein in planta. J Gen Virol **85:** 1055–1063

Ligat L, Lauber E, Albenne C, San Clemente H, Valot B, Zivy M, Pont-Lezica R, Arlat M, Jamet E (2011) Analysis of the xylem sap proteome of *Brassica oleracea* reveals a high content in secreted proteins. Proteomics **11:** 1798–1813

Lionetti V, Raiola A, Cervone F, Bellincampi D (2014a) How do pectin methylesterases and their inhibitors affect the spreading of tobamovirus? Plant Signal Behav **9:** e972863

Lionetti V, Raiola A, Cervone F, Bellincampi D (2014b) Transgenic expression of pectin methylesterase inhibitors limits tobamovirus spread in tobacco and Arabidopsis. Mol Plant Pathol **15:** 265–274

Longatti A (2015) The dual role of exosomes in hepatitis A and C virus transmission and viral immune activation. Viruses **7:** 6707–6715

Lucocq JM, Habermann A, Watt S, Backer JM, Mayhew TM, Griffiths G (2004) A rapid method for assessing the distribution of gold labeling on thin sections. J Histochem Cytochem **52:** 991–1000

Macho AP, Zipfel C (2014) Plant PRRs and the activation of innate immune signaling. Mol Cell **54:** 263–272

Masciopinto F, Giovani C, Campagnoli S, Galli-Stampino L, Colombatto P, Brunetto M, Yen TS, Houghton M, Pileri P, Abrignani S (2004) Association of hepatitis C virus envelope proteins with exosomes. Eur J Immunol **34:** 2834–2842

McMullen CR, Gardner WS, Myers GA (1977) Ultrastructure of cell-wall thickenings and paramural bodies induced by barley stripe mosaic-virus. Phytopathology **67:** 462–467

Meyer D, Pajonk S, Micali C, O'Connell R, Schulze-Lefert P (2009) Extracellular transport and integration of plant secretory proteins into pathogen-induced cell wall compartments. Plant J **57:** 986–999

Movahed N, Patarroyo C, Sun J, Vali H, Laliberté JF, Zheng H (2017) Cylindrical inclusion protein of turnip mosaic virus serves as a docking point for the intercellular movement of viral replication vesicles. Plant Physiol **175:** 1732–1744

Nielsen ME, Feechan A, Böhlenius H, Ueda T, Thordal-Christensen H (2012) Arabidopsis ARF-GTP exchange factor, GNOM, mediates transport required for innate immunity and focal accumulation of syntaxin PEN1. Proc Natl Acad Sci USA **109:** 11443–11448

Pegtel DM, Peferoen L, Amor S (2014) Extracellular vesicles as modulators of cell-to-cell communication in the healthy and diseased brain. Philos Trans R Soc Lond B Biol Sci **369:** 20130516

Perez-Hernandez D, Gutiérrez-Vázquez C, Jorge I, López-Martín S, Ursa A, Sánchez-Madrid F, Vázquez J, Yáñez-Mó M (2013) The intracellular interactome of tetraspanin-enriched microdomains reveals their function as sorting machineries toward exosomes. J Biol Chem **288:** 11649–11661

Regente M, Corti-Monzón G, Maldonado AM, Pinedo M, Jorrín J, de la Canal L (2009) Vesicular fractions of sunflower apoplastic fluids are associated with potential exosome marker proteins. FEBS Lett **583:** 3363–3366

Restrepo-Hartwig MA, Carrington JC (1994) The tobacco etch potyvirus 6-kilodalton protein is membrane associated and involved in viral replication. J Virol **68:** 2388–2397

Rutter BD, Innes RW (2017) Extracellular vesicles isolated from the leaf apoplast carry stress-response proteins. Plant Physiol **173:** 728–741

Ryabova L, Park HS, Hohn T (2004) Control of translation reinitiation on the cauliflower mosaic virus (CaMV) polycistronic RNA. Biochem Soc Trans **32:** 592–596

Shurtleff MJ, Temoche-Diaz MM, Karfilis KV, Ri S, Schekman R (2016) Y-box protein 1 is required to sort microRNAs into exosomes in cells and in a cell-free reaction. eLife **5:** e19276

Thivierge K, Cotton S, Dufresne PJ, Mathieu I, Beauchemin C, Ide C, Fortin MG, Laliberté JF (2008) Eukaryotic elongation factor 1A interacts with turnip mosaic virus RNA-dependent RNA polymerase and VPg-Pro in virus-induced vesicles. Virology **377:** 216–225

Uchiyama A, Shimada-Beltran H, Levy A, Zheng JY, Javia PA, Lazarowitz SG (2014) The Arabidopsis synaptotagmin SYTA regulates the cell-to-cell movement of diverse plant viruses. Front Plant Sci **5:** 584

Wan J, Laliberté JF (2015) Membrane-associated virus replication complexes locate to plant conducting tubes. Plant Signal Behav **10:** e1042639

Wan J, Cabanillas DG, Zheng H, Laliberté JF (2015) Turnip mosaic virus moves systemically through both phloem and xylem as membrane-associated complexes. Plant Physiol **167:** 1374–1388

Wang RY, Nagy PD (2008) Tomato bushy stunt virus co-opts the RNA-binding function of a host metabolic enzyme for viral genomic RNA synthesis. Cell Host Microbe **3:** 178–187

Wang F, Shang Y, Fan B, Yu JQ, Chen Z (2014) Arabidopsis LIP5, a positive regulator of multivesicular body biogenesis, is a critical target of pathogen-responsive MAPK cascade in plant basal defense. PLoS Pathog **10:** e1004243

Wang J, Ding Y, Wang J, Hillmer S, Miao Y, Lo SW, Wang X, Robinson DG, Jiang L (2010) EXPO, an exocyst-positive organelle distinct from multivesicular endosomes and autophagosomes, mediates cytosol to cell wall exocytosis in Arabidopsis and tobacco cells. Plant Cell **22:** 4009–4030

Wang J, Wang XR, Zhou Q, Yang JM, Guo HX, Yang LJ, Liu WQ (2016) iTRAQ protein profile analysis provides integrated insight into mechanisms of tolerance to TMV in tobacco (*Nicotiana tabacum*). J Proteomics **132:** 21–30

Wei T, Hibino H, Omura T (2009) Release of Rice Dwarf Virus from insect vector cells involves secretory exosomes derived from multivesicular bodies. Commun Integr Biol **2:** 324–326

Willms E, Johansson HJ, Mäger I, Lee Y, Blomberg KE, Sadik M, Alaarg A, Smith CI, Lehtiö J, El Andaloussi S, et al (2016) Cells release subpopulations of exosomes with distinct molecular and biological properties. Sci Rep **6:** 22519

Xu JY, Chen GH, Yang YJ (2017) Exosomes: A rising star in falling hearts. Front Physiol **8:** 494

Yang Y, Han Q, Hou Z, Zhang C, Tian Z, Zhang J (2017) Exosomes mediate hepatitis B virus (HBV) transmission and NK-cell dysfunction. Cell Mol Immunol **14:** 465–475

Zheng H, Kunst L, Hawes C, Moore I (2004) A GFP-based assay reveals a role for RHD3 in transport between the endoplasmic reticulum and Golgi apparatus. Plant J **37:** 398–414